Field theoretic and Monte Carlo analysis of the Domb - Joyce model

1997 J. Phys. A: Math. Gen. 30 7039

(http://iopscience.iop.org/0305-4470/30/20/010)

J. Phys. A: Math. Gen. **30** (1997) 7039–7056. Printed in the UK PII: S0305-4470(97)83411-7

Field theoretic and Monte Carlo analysis of the Domb–Joyce model

Peter Grassberger†, Peter Sutter‡ and Lothar Schäfer‡

† Physics Department, University of Wuppertal, D-42097 Wuppertal, Germany and HLRZ c/o Forschungszentrum Jülich, D-52425 Jülich, Germany

‡ Physics Department, University of Essen, D-45117 Essen, Germany

Received 14 April 1997

Abstract. We present a field-theoretic analysis of high-precision Monte Carlo data for the Domb–Joyce model on the sc lattice. We vary the repulsion between two segments at the same point from zero (random walk) to infinity (self-avoiding walk). Eventually, we even include a repulsion between segments at neighbour points to increase the excluded volume beyond that of self-avoiding walks. The data for the end-to-end distance, the radius of gyration and the partition function clearly show the existence of two branches of universal behaviour. These two branches can be identified with the weak- and strong-coupling branch of the renormalization group, respectively. A quantitative analysis shows the ability of the standard field theoretic approach to describe the data, including the data for strong coupling, i.e. renormalized coupling u greater than its fixed point value u^*. We conclude, in contrast with some claims in the literature, that the standard formalism of the renormalized field theory can be used even for $u > u^*$ (strong-coupling branch). In addition, exploiting the fast approach to asymptotic behaviour at the transition between weak and strong coupling, we obtain very precise estimates for the critical exponents of self-avoiding walks.

1. Introduction

Thermodynamic systems at a critical point, like ferromagnets at the Curie point or infinitely dilute solutions of infinitely long polymer chains, show simple power-law and scaling behaviour. For a given class of systems this behaviour is universal, i.e. independent of details of the microstructure. It can be understood within the frame of field theory and of the renormalization group, which describes the change of the field theoretic model under a dilatation of the elementary length scale. The critical point corresponds to a fixed point of the renormalization group. Here the theory becomes scale invariant, and universal power and scaling laws result.

On the quantitative level the standard renormalized field theory has provided estimates of universal fixed-point quantities, which are in good agreement with the experimental data [1]. However, the corrections to that limiting behaviour sometimes even qualitatively differ from field theoretic predictions found in the literature [2–4]. The amplitudes of these 'corrections to scaling' have the wrong sign. Well known examples are the susceptibility of the three-dimensional Ising model [2] or the end-to-end distance of strictly self-avoiding walks (SAWs) on typical three dimensional lattices [4]. In both cases the asymptotic power-law behaviour is approached from a direction opposite to that predicted by field theory. Therefore, the applicability of the theory to these systems has been questioned [2, 4, 5].

0305-4470/97/207039+18$19.50

Within the framework of field theory the corrections to scaling are proportional to the deviation $(u^* - u)$ of the renormalized coupling u from its fixed point value $u^* > 0$. The theory proceeds by expansion about $u = 0$, and the standard predictions for the corrections to scaling are derived in the continuum limit of the theory. This leads to the restriction $u \leqslant u^*$ which fixes the sign of the corrections. The empirical observation of corrections to scaling of opposite sign then raises the question whether the field theoretic results can be analytically continued to $u > u^*$. As we are dealing with systems which have a finite microscopic cut-off (the lattice spacing of the ferromagnet or the segment size of the polymer, respectively), arguments based on the continuum limit which enforces the restriction $u \leqslant u^*$ do not apply. Contradictory statements on that issue are found in the literature, but a careful review of the field theoretic approach [6–8] shows that there is neither a proof nor a disproof of the validity of the field theory for $u > u^*$ in problems of statistical mechanics. We therefore consider here, on an empirical level, the question whether results of renormalized field theory, applied at $u > u^*$, are supported by experiment. Specifically we analyse self-repelling walk data taken for various strengths of the self repulsion, which directly influences the renormalized coupling u. Our work extends previous studies, where simulation data for the end-to-end distance R_e of self-repelling walks [8] or physical solution data for the radius of gyration R_g and the second viral coefficient A_2 [9] have been analysed.

We briefly explain the general theoretical structure with the example of the end-to-end distance. Renormalized field theory predicts a scaling form as a function of the self repulsion ('excluded volume strength') and chain length N (number of steps in the walk):

$$R_e = \sqrt{2d\tilde{l}}N^{1/2}\tilde{\alpha}_e(\tilde{z}) \tag{1}$$

$$\tilde{z} = \tilde{v}N^{1/2}. \tag{2}$$

The nonuniversal parameters $\tilde{l}$, $\tilde{v}$ depend on the step length, the excluded volume, and on other microscopic features of the model. The critical limit is reached for $\tilde{z} \to \infty$, where $\tilde{\alpha}_e$ reduces to a universal power law,

$$\tilde{\alpha}_e(\tilde{z}) \underset{\tilde{z}\to\infty}{\longrightarrow} a_e\tilde{z}^{2\nu-1} \tag{3}$$

where ν is the correlation length exponent. The function $\tilde{\alpha}_e(\tilde{z})$ for $\tilde{z} < \infty$ describes the correction to scaling. It is universal and can be calculated as a power series in terms of the renormalized coupling u. Perturbation theory also enters in a second step, well separated from the perturbative determination of the scaling functions. It is used to establish the renormalization group (RG) flow equations which give the change of the renormalized theory under an infinitesimal dilatation. Integrating these equations we find two branches, depending on the starting point of the flow. For systems close to θ conditions, where on microscopic scales the effect of the self repulsion is small, we find the weak-coupling branch $\tilde{\alpha}_e^{(<)}(\tilde{z})$, corresponding to $u < u^*$. For large self-repulsion, however, we reach the strong-coupling branch $\tilde{\alpha}_e^{(>)}(\tilde{z})$, where $u > u^*$. In the excluded volume limit $\tilde{z} \to \infty$ both branches approach the same asymptotic power law (3), coming, however, from opposite sides (see figure 1).

Previous work by one of us [8] indeed uncovered this two-branched structure in Monte Carlo (MC) data, but the data basis was not very large. In particular, the range of $\tilde{z}$ for different values of the excluded volume did not overlap, so that the universal scaling feature predicted by the theory could not be tested. Furthermore, for each excluded volume strength the theory involves two fit parameters $\tilde{v}$, $\tilde{l}$, so that fitting a single observable is not a strong test of the quantitative reliability of the theory. Likewise, the analysis of solution physical data [9] was consistent with the two-branched structure, but the accuracy of the data was by far insufficient for any quantitative test.

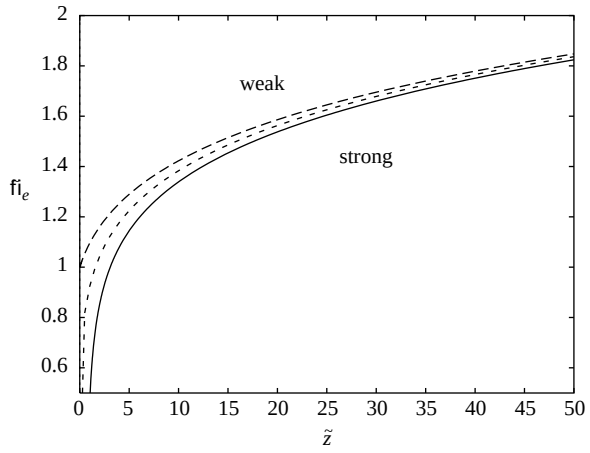

Figure 1. The scaling function $\tilde{\alpha}_e$ as a function of $\tilde{z}$. Middle curve asymptotic.

This situation asks for new high-precision simulations, covering a large range of chain length and excluded volume strength. Since for a given excluded volume all observables involve the same two parameters $\tilde{l}$,$\tilde{v}$, we should measure several observables and compare the results to the quantitative predictions of field theory. In our simulation we used the Domb–Joyce model [10] on a simple cubic lattice, employing an improved chain-growth algorithm [11, 12]. We systematically varied the on-site repulsion, acting if two monomer positions coincide, but to enlarge the excluded volume we eventually also included and varied a nearest-neighbour repulsion. The chain length extends up to $N = 1.6 \times 10^4$, depending on the interaction strength. We measured the end-to-end distance, the radius of gyration, the partition function, and the average value and the variance of the potential energy. In the present paper we present a detailed analysis of the first three variables, the latter two being analysed elsewhere [13]. For each observable the data clearly exhibit a two-branched scaling structure, thus supporting our qualitative expectation.

The quantitative comparison of the MC data and RG calculation was performed in several steps. In a first step, we have to convince ourselves that the data are mutually consistent (e.g. the mean energy should be related to the derivative of the partition function with respect to the interaction strength), and that all data asymptotically tend to the SAW fixed point. For that we performed phenomenological fits and made precise estimates of effective critical exponents. Next, we have to map the Domb–Joyce model onto field theory. This involves nonuniversal parameters which are considered as fitting parameters. In particular, this involves finding that value of the Domb–Joyce coupling which corresponds to the transition from weak to strong coupling. We obtained these parameters from a single observable, the end-to-end distance. Finally, given all these nonuniversal parameters, we are able to predict the variation of the other measured quantities, namely the radius of gyration and the partition function. We find good agreement among theory and data.

2. Summary of theoretical results

We consider a discrete chain model, composed of $N + 1$ segments connected by N bonds of average size of order ℓ. The configuration of the chain is described by $N + 1$ segment

coordinates $\boldsymbol{r}_j$, $j = 0, \ldots, N$ in d-dimensional space ($\boldsymbol{r}_0 = 0$). The Hamiltonian is given by

$$\mathrm{e}^{-\mathcal{H}/k_BT} = \exp\left\{ -\frac{1}{4\ell^2}\sum_{j=1}^{N}(\boldsymbol{r}_j - \boldsymbol{r}_{j-1})^2 \right\} \prod_{(j,k)}{}' [1 - (4\pi\ell^2)^{d/2}\beta_e \delta^d(\boldsymbol{r}_j - \boldsymbol{r}_k)] \tag{4}$$

where $\beta_e \geqslant 0$ is the dimensionless excluded-volume parameter. The product extends over all pairs (j, k) of segments indices, with the restriction that in the cluster expansion all terms where any segment index occurs more than once are omitted. The partition function is given by integration over all segment coordinates

$$\mathcal{Z}(N) = \int_\Omega D[r]\, \mathrm{e}^{-\mathcal{H}/k_BT} \tag{5}$$

and the end-to-end distance R_e and the radius of gyration R_g are defined as

$$R_e^2 = \langle(\boldsymbol{r}_N - \boldsymbol{r}_0)^2\rangle \qquad R_g^2 = \frac{1}{N+1}\left\langle \sum_{i=0}^{N}(\boldsymbol{r}_i - \boldsymbol{R}_{\mathrm{CM}})^2 \right\rangle \tag{6}$$

where $\boldsymbol{R}_{\mathrm{CM}}$ is the centre of mass.

The model has to be evaluated perturbatively. All quantities are calculated in the cluster expansion in powers of β_e. For the regime of interest, $\beta_e > 0$ and N large, the bare expansion parameter $z \sim \beta_e N^{1/2}$ diverges. This well known problem is solved by renormalization, which means that there exists a mapping from the 'bare' parameters ℓ, N and β_e to the renormalized counterparts ℓ_R, n_R and u changing physical observables only by terms of (canonical) order $1/N$. For sufficiently large N the effects of order $1/N$ should be negligible.

The renormalized segment size ℓ_R can be chosen arbitrarily, so that renormalization yields a one-parameter family $(\ell_R, u(\frac{\ell_R}{\ell}), n_R(\frac{\ell_R}{\ell}))$ of renormalized theories, all equivalent to the given bare theory up to corrections of order $1/N$. The renormalization group mapping $(\ell, \beta_e, N) \to (\ell_R, u, n_R)$ is known with good precision from high-order calculations. We here employ a form established within the framework of the 'minimal subtraction' scheme. In three dimensions this mapping has been determined numerically, and we here use an analytical parametrization of the results that respects the basic analytic structure and reproduces the results within the numerical accuracy of these previous analyses [8, 14],

$$\ell_R = f|1-f|^{-1/\omega}(1 + 0.824f)^{0.25}\frac{\tilde{l}}{\tilde{v}} \tag{7}$$

$$n_R = f^{-2}|1-f|^{1/(\omega\nu)}\frac{1 - 0.005f - 0.028f^2 + 0.022f^3}{\sqrt{1+0.824f}}\,\tilde{v}^2 N \tag{8}$$

$$f = u/u^*. \tag{9}$$

Here the values $\nu = 0.588$, $\omega = 0.80$ and $u^* = 0.364$ have been used [17, 18]. We will thus also use these values in the comparison with field theory, although MC estimates with supposedly higher accuracy exist [4], and although we shall argue that our own MC data also give estimates for ν and ω (and, in particular, γ) with higher precision. However, our first-order evaluation of the scaling functions is not so precise as to seriously consider the small difference among the above-quoted values and the MC estimates.

The parameters $\tilde{l}$ and $\tilde{v}$ are functions of $f_0 = \frac{u(\ell_R=\ell)}{u^*}$, which has a nontrivial but analytical dependence on the excluded volume parameter β_e. These two nonuniversal microscopic parameters will be considered as fit parameters.

The renormalization group mapping (7), (8) shows two different branches depending upon the starting point f_0. For $0 \leqslant f_0 < 1$ we always find $f < 1$, corresponding to the weak-coupling branch. Starting with $f_0 > 1$ we have $f > 1$ corresponding to the strong-coupling branch.

Within the renormalized theory we can now determine the physical quantities by an expansion in powers of u. Our results for the end-to-end distance, the radius of gyration and the partition function are based on first-order renormalized perturbation theory. We find [15, 16]

$$R_e^2 = 2d\ell_R^2 n_R \left[1 + u\left\{n_R^{\epsilon/2}\frac{2}{\epsilon(2+\epsilon)} - \frac{1}{\epsilon}\right\} + \mathcal{O}(u^2)\right] \tag{10}$$

$$R_g^2 = \frac{d}{3}\ell_R^2 n_R \left[1 + u\left\{\frac{1}{2}n_R^{\epsilon/2}\left(\frac{2}{\epsilon} - \frac{2}{2+\epsilon} - \frac{1}{4+\epsilon} + \frac{1}{6+\epsilon}\right) - \frac{1}{\epsilon}\right\} + \mathcal{O}(u^2)\right]$$

where $\epsilon = 4 - d$. The partition function $\mathcal{Z}(N)$ is given by

$$\mathcal{Z}(N) = \frac{\Omega}{(4\pi\ell^2)^{d/2}}\,\mathrm{e}^{\mu^* N}\,\frac{Z(u)}{Z_N(u)}\left[1 + u\left\{n_R^{\epsilon/2}\left(\frac{1}{\epsilon} + \frac{1}{2-\epsilon}\right) - \frac{1}{\epsilon}\right\} + \mathcal{O}(u^2)\right] \tag{11}$$

where $Z(u)$, $Z_N(u)$ are standard renormalization factors. μ^* is the chemical potential per segment of an infinitely long chain.

In evaluating such expressions we first have to fix the arbitrary scale ℓ_R. As mentioned above, in the theory evaluated to *all* orders, ℓ_R is arbitrary, but in a low-order approximation the choice of ℓ_R matters. It has to be chosen so as to enforce a good expansion scheme. Now u^* in three dimensions is reasonably small. Since the expansions involve powers of $un_R^{\epsilon/2}$, this suggests the choice of $n_R = n_0 = \mathcal{O}(1)$, implying $\ell_R = \mathcal{O}(R_g)$. In other words, we choose ℓ_R to be of the order of the relevant macroscopic length scale. To fix $n_R = n_0$ precisely we consider the fixed-point value of some universal ratio, which is most sensitive to n_R. A good choice is the interpenetration ratio ψ, which is constructed from the second viral coefficient and the radius of gyration

$$\psi = \left(\frac{d}{12\pi}\right)^{d/2}\frac{A_2}{R_g^d}. \tag{12}$$

To one-loop order it reads

$$\psi = \frac{u}{2}n_R^{\frac{4-d}{2}}\,\frac{\left[1 + \frac{2u}{\epsilon}\left(1 - n_R^{\epsilon/2}\frac{6+\epsilon-2^{2+\epsilon/2}}{(1-\epsilon^2/4)(2+\epsilon/2)}\right)\right]}{\left[1 - \frac{u}{\epsilon} + \frac{u}{2}n_R^{\epsilon/2}\left(\frac{2}{\epsilon} - \frac{2}{2+\epsilon} - \frac{1}{4+\epsilon} + \frac{1}{6+\epsilon}\right)\right]^{d/2}}. \tag{13}$$

At the fixed point it takes a universal value ψ^*. If we keep the n_0 dependence, ψ^* is given by ($d = 3$, $u^* = 0.364$)

$$\psi^* = 0.182\sqrt{n_0}\,\frac{1.728 - 0.521\sqrt{n_0}}{\left(0.636 + 0.232\sqrt{n_0}\right)^{3/2}}. \tag{14}$$

For $n_0 \approx 1$, ψ^* is insensitive to n_0 and we will choose n_0 such that ψ^*, in this approximation, is equal to the experimental value $\psi^*_{\mathrm{exp}} = 0.245$ [20, 3, 19]. This leads to $n_0 = 0.53$. We should note that our final results for R_e etc are quite insensitive to the choice of n_0, as long as $n_0 = \mathcal{O}(1)$. The main effect of a variation of n_0 is absorbed into the nonuniversal parameters $\tilde{v}$, $\tilde{l}$.

We are now in a position to discuss the structure of our results. We again use the example of the end-to-end distance, discussing the swelling factor

$$\tilde{\alpha}_e^2(\tilde{z}) = \frac{R_e^2}{2d\tilde{l}^2 N}. \tag{15}$$

Consider first the limit $f \to 0$. For $d = 3$, equation (10) yields

$$\begin{aligned}\tilde{\alpha}_e^2 &= [1 + \tilde{a}_0 f + \cdots] \\ &= [1 + a_0\tilde{v}\sqrt{N} + \cdots]\end{aligned} \tag{16}$$

which is the result for a random walk (RW) including the first correction due to the excluded volume. In this regime $\tilde{v}$ is proportional to the bare excluded volume strength $\tilde{v} \sim \beta_e$ and the additional parameter $\tilde{l}$ is equal to the microscopic length $\tilde{l} = \ell$.

Increasing $f \to 1$ we trace out the weak-coupling branch. In the excluded volume regime, $f \approx 1$, we find

$$\begin{aligned} \tilde{\alpha}_e^2 &= CN^{2\nu-1}[1 + \tilde{a}_s(1-f) + \cdots] \\ &= CN^{2\nu-1}[1 + a_s(\tilde{v}\sqrt{N})^{-2\omega\nu} + \cdots] \end{aligned} \tag{17}$$

where $C = C(\tilde{v})$ is a constant. The correction-to-scaling amplitude a_s is positive for $f < 1$. Evaluating the theory also for $f > 1$ we construct the strong-coupling branch, where a_s is *negative*. Figure 1 illustrates these results. Clearly the two-branched structure of the RG mapping induces a two-branched structure for all observables.

Equations (7) and (8) give the RG mapping in an implicit form, which is not very practical for an analysis of data. We therefore evaluated the theory numerically in $d = 3$ and parametrized the results by simple analytical expressions. Specifically we evaluated the end-to-end swelling $\tilde{\alpha}_e^2$ (equation 15), the corresponding quantity for the radius of gyration

$$\tilde{\alpha}_g^2(\tilde{z}) = \frac{3}{d}\frac{R_g^2}{\tilde{l}^2 N} \tag{18}$$

as well as a function $F(\tilde{z})$ defined by

$$C(N) = \frac{\mathcal{Z}(N)}{\mathcal{Z}(1)} = \mathrm{e}^{\mu^*(N-1)} N^{(\gamma-1)} \frac{F(\tilde{z})}{F(\tilde{v})} \tag{19}$$

where $\gamma \approx 1.158$ ($d = 3$) is another asymptotic exponent. All these functions depend only on the variable $\tilde{z} = \tilde{v}N^{1/2}$ (equation 2). We find simple parametrizations (in $d = 3$):

$$\begin{aligned} \tilde{\alpha}_e^2(\tilde{z}) &= \begin{cases} (1.00 + 1.40\tilde{z} + 0.40\tilde{z}^2)^{(2\nu-1)} & : \text{weak} \\ 0.851\tilde{z}^{2(2\nu-1)}(1.00 - 0.53\tilde{z}^{-2\nu\omega} - 0.2247\tilde{z}^{-1-2\nu\omega}) & : \text{strong} \end{cases} \\ \tilde{\alpha}_g^2(\tilde{z}) &= \begin{cases} (1.00 + 1.32\tilde{z} + 0.378\tilde{z}^2)^{(2\nu-1)} & : \text{weak} \\ 0.843\tilde{z}^{2(2\nu-1)}(1.00 - 0.54\tilde{z}^{-2\nu\omega} - 0.2376\tilde{z}^{-1-2\nu\omega}) & : \text{strong} \end{cases} \\ F(\tilde{z}) &= \begin{cases} (4.3633 + 4.578\tilde{z}^{-1} + 1.0\tilde{z}^{-2})^{(\gamma-1)} & : \text{weak} \\ 1.2627(1.00 - 0.1411\tilde{z}^{-2\nu\omega} + 0.0312\tilde{z}^{-4\nu\omega}) & : \text{strong.} \end{cases} \end{aligned} \tag{20}$$

Note that these parametrizations are not meant to incorporate the full analytic structure predicted by the renormalization group. In particular in the excluded volume limit $\tilde{z} \to \infty$ they only reproduce the leading power (weak coupling) or the first two leading powers (strong coupling) of the full theoretical results. They merely numerically reproduce the full results within 1% deviation, which is adequate within our one-loop approximation.

The errors due to neglecting higher-order loops are of course not known in detail, but one relatively large error is well documented [21] and worth mentioning. The ratio $\tilde{\alpha}_g^2/\tilde{\alpha}_e^2$ is predicted wrongly by $\approx 3\%$. For $\tilde{z} = \infty$ it is ≈ 0.96 [18, 4], while equation (20) would predict 0.99. Since this ratio is 1 in the RW limit, this error exceeds the total variation over the entire weak-coupling branch. Thus we should not use equation (20) for detailed comparison with MC data for this ratio.

We should also comment on the parametrization for the weak-coupling branch, as one might wonder why we did not employ the same analytic structure as for the strong-coupling branch. The latter would follow more closely the correct analytic behaviour for large $\tilde{z}$, but it would be completely inappropriate for $\tilde{z} \to 0$. The advantage of the parametrization chosen in equation (20) is that it gives a good numerical fit over the entire range of $\tilde{z}$.

Finally, we should comment on nonuniversal corrections which are not included in equation (20). Such corrections are due to chain stiffness, three-body forces, etc. Taking into account the leading correction to R_e^2 in the weak-coupling branch, e.g. we would roughly obtain

$$R_e^2/N = 2d\tilde{l}^2\tilde{\alpha}_e^2(\tilde{z})\left(1 + \frac{B(\tilde{v})}{N}\right) \tag{21}$$

with an unknown and nonuniversal amplitude $B(\tilde{v})$. (More precisely, close to the excluded volume limit the renormalization group predicts several corrections of the form $\mathcal{O}(1/N^{x_j})$ with $x_j \approx 1$.) Although the last term has a completely different origin, it cannot be uniquely separated from the $1/\tilde{z}^2$ term in the expansion $\tilde{\alpha}_e^2 = 0.85\tilde{z}^{2(2\nu-1)}(1+0.62/\tilde{z}+0.72/\tilde{z}^2+\cdots)$. The only exceptions are for the neighbourhood of the RW limit ($\tilde{z} \to 0$) and precisely at the weak/strong cross-over point. There we have $\tilde{z} = \infty$, whence all deviations from perfect scaling are due to nonuniversal corrections. Away from these points, all we can do is to hope that the function $B(\tilde{v})$ is smooth and not too large. Thus the numerical test of the above theory consists in showing that the rest remaining after subtraction of the theoretical predictions has indeed these features. The same remark of course also holds for the other observables, and for higher-order $(1/N^2, 1/N^3, \ldots)$ correction terms.

3. Monte Carlo analysis

3.1. Simulations and data

We consider a slight extension of the original Domb–Joyce model [10]. The model is defined on a simple cubic lattice. The partition function for a chain of length N is given by the weighted sum over all N-step RW configurations

$$Z(N) = \sum_{\text{config.}} (1-w)^{\kappa_1}(1-q)^{\kappa_2} \tag{22}$$

where κ_1 is the number of the crossings of the walk and κ_2 is the number of (nonbonded) nearest-neighbours (nN). Crossings are weighted according to their multiplicity, i.e. a point with m visits of the walk contributes a factor $(1-w)^{m(m-1)/2}$. The case $w = 0$, $q = 0$ corresponds to the RW, $w = 1$, $q = 0$ to the SAW, and $w = 1$, $q = 1$ to a walk with no nN. Systematically varying w and q we can interpolate among these limits. We actually used $q \neq 0$ only together with $w = 1$, i.e. used nN repulsion only to increase the excluded volume effect beyond that of ordinary SAWs. For $q = 0$ our model is identical to the Domb–Joyce model.

In addition to data for $w < 1$ resp. $q \neq 0$, we present also new high-statistics data for $w = 1, q = 0$, i.e. for SAWs. It is accepted that the most efficient algorithm in this case is the pivot algorithm [4, 22], provided one is not interested in the partition sum itself but only in configurational properties (R_e, R_g, $\langle E \rangle, \ldots$). We thus performed additional simulations with the pivot algorithm for intermediate chain lengths ($100 < N < 9000$) where previous analyses [4, 23–25] had relatively poor statistics. In these simulations we measured only R_e. The results are given in table 1.

For the bulk of the simulations we used chain-growth algorithms as described in detail in [11, 12]. The reasons for not using the pivot algorithm are mainly the following.

- Estimating partition sums is not easy with the pivot algorithm. There exist modifications of the pivot algorithms for this purpose [26], but they do not seem to be easy to implement or very efficient (see note added in proof).
- The efficiency of the pivot algorithm for SAWs results mainly from the fact that most 'wrong' moves leading to intersections are detected very soon. Thus it is not too costly

Table 1. End-to-end distances and sample sizes for SAW simulations using the pivot algorithm.

N	R_e^2/N	Number of pivot moves
104	$2.671\,30 \pm 0.000\,10$	5.08×10^9
208	$3.042\,10 \pm 0.000\,12$	6.14×10^9
300	$3.255\,10 \pm 0.000\,13$	5.74×10^9
416	$3.455\,94 \pm 0.000\,16$	4.96×10^9
832	$3.920\,00 \pm 0.000\,29$	2.90×10^9
1200	$4.187\,45 \pm 0.000\,40$	1.54×10^9
2000	$4.589\,11 \pm 0.000\,56$	9.64×10^8
4000	$5.192\,21 \pm 0.000\,75$	8.54×10^8
6000	$5.579\,56 \pm 0.000\,80$	8.66×10^8
9000	$5.991\,34 \pm 0.001\,53$	2.82×10^8

to try many unaccepted moves. This is different for the Domb–Joyce model, where the acceptance of a pivot move is determined by a Metropolis (or heat bath) criterion which needs the entire move to be performed in each case. Thus one loses the main advantage as soon as $w < 1$.

• The efficiency of the algorithms of [11, 12] is greatly increased when $w \ll 1$ and $q = 0$. In these algorithms, monomers are added to and taken away from the end of a partial chain so that the chain length N performs essentially a RW. Thus it takes roughly $\approx N^2/D$ MC steps to generate one independent chain of length N, with D being the effective diffusion coefficient. In the limit $w \to 0$ one finds $D \propto 1/w$. Thus for our smallest value of w (=0.00125), we were able to make chains with length 10^4 essentially in time $\mathcal{O}(N)$.

An important feature of the algorithms of [11, 12] is that they generate data for all N less then some prescribed $N_{\max}$. But these data are not independent, thus making least-square fits rather delicate (unless we estimate the full covariance matrix, which is not feasible for the present chain lengths). Also, successive chains are not produced independently. Instead, they are produced in bunches (called 'tours' in [11, 12]) such that chains within one tour are correlated, while chains in different tours are strictly independent. Thus the number of tours which have reached a length N is a direct measure of the number of independent chains of this length. It is a better indicator of statistical significance than the total number of chains generated. The characterization of the data set is given in table 2.

3.2. Numerical results and heuristic analysis

We do not show numerical results of the observables themselves. Such plots would not be informative, the statistical errors being much smaller than any symbol sizes or line widths. A first alternative to showing raw data consists in showing ratios between them and analytic fits. If the fit is perfect, then the plot should be flat. As an example we show in figure 2 SAW data for R_e^2/N. In addition to our own (pivot- and chain-growth) data we also include results from [4, 23]. We see that all data are compatible within the error bars. The fit, taken at face value, would give $\nu = 0.586\,84$ and $\Delta \equiv \omega\nu = 0.4$. It is hard to attribute error bars to these values, as the errors would be largely systematic due to the uncertainty in the analytical form of the parametrization. As usual in MC analyses, this gives a large error for Δ. Thus our value of Δ is compatible with the somewhat higher estimate from field theory, but the estimate $\Delta = 0.56 \pm 0.03$ from [4] seems too high. The fit used in figure 2 involves $1/N$ corrections and higher terms. From this fit alone we cannot decide whether

Table 2. Sample characteristics for MC data using chain-growth algorithms.

w	q	$N_{\max}$	Number of chains	Number of tours reaching $N_{\max}$
1	1	2 000	2.2×10^6	96 146
1	0.4	2 000	3.7×10^6	270 720
1	0.2	2 000	6.5×10^6	524 755
1	0	4 000	1.2×10^9	3689 104[a]
0.8	0	2 000	1.1×10^8	1260 544
0.6	0	2 500	1.3×10^8	1227 452
0.5	0	2 500	2.2×10^8	2183 117
0.4	0	3 000	2.2×10^8	2705 814
0.3	0	4 000	1.0×10^8	843 811
0.2	0	5 000	4.9×10^7	298 157
0.1	0	4 000	2.1×10^7	407 649
0.05	0	4 000	2.1×10^7	612 399
0.02	0	8 000	1.0×10^7	337 961
0.01	0	8 000	7.5×10^6	362 272
0.005	0	8 000	6.6×10^6	632 932
0.002 5	0	15 942	4.7×10^6	479 403
0.001 25	0	15 000	3.1×10^6	570 859

[a] R_g was measured only for $\sim 2\%$ of these data.

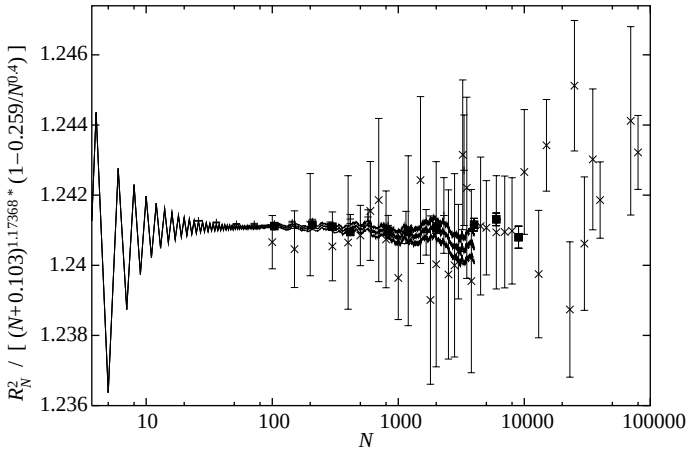

Figure 2. SAW data for R_e^2 divided by a fit $R_{e,\mathrm{fit}}^2$ as a function of N. The fit is $R_{e,\mathrm{fit}}^2 = (N + 0.103)^{2\nu}(1 - 0.259N^{-0.4})$ with $\nu = 0.586\,84$. $\times$, SAW data from [4], $+$, data from [23]; ■, our pivot data. The central curve is from our chain-growth simulations, with the broken lines giving the error bars.

these are indeed analytic corrections or rather universal corrections $\sim 1/N^{2\omega\nu}$. Also, such corrections render an estimate of Δ unstable.

An analogous plot for Z_N is shown in figure 3. We have used a parametrization which is compatible with $\Delta = 0.5$; again the error is hard to estimate. Our estimate for γ, on the other hand, seems to be quite robust, giving us a preliminary $\gamma = 1.157 \pm 0.001$. This agrees perfectly with the (less precise) field theoretic estimate [17], but is much smaller than most other estimates from simulations [28] and from exact enumerations [27] (see note added in proof).

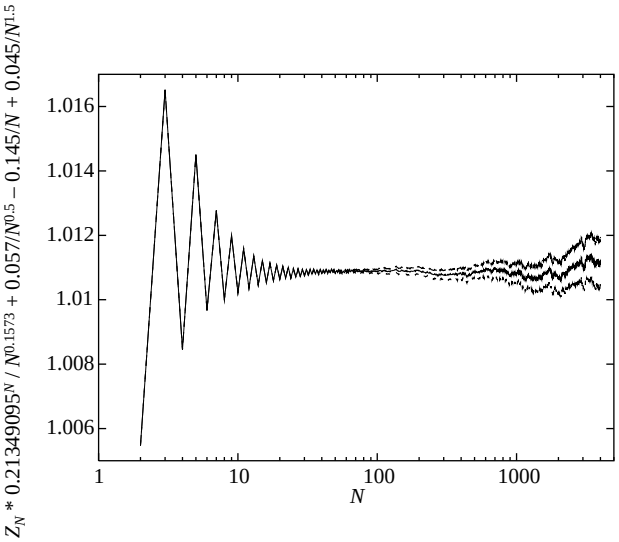

Figure 3. SAW data for Z_N as a function of N as determined by the chain-growth algorithm. More precisely, the central curve gives $Z_N/[e^{\mu N}N^{\gamma-1}] + a/\sqrt{N} + b/N + c/N^{3/2}$ with $\mu = 1.544\,1608$, $\gamma = 1.1573$, $a = 0.057$, $b = -0.145$, $c = 0.045$. Broken lines give error bars.

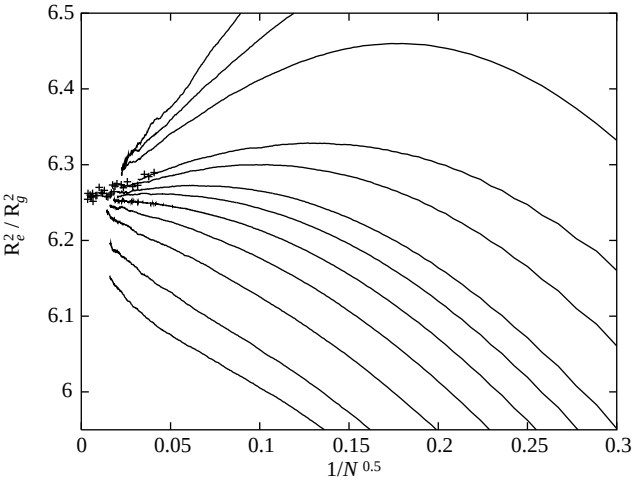

Figure 4. The ratio R_e^2/R_g^2 for different w, q. From above: $q = 1.0, 0.4, 0.2$ and $w = 1.0$; then $w = 1.0, \ldots, 0.05$ and $q = 0$. $+$, SAW data from [4].

We have made analogous fits for other observables, and for other values of w and q. In general the exponents are compatible with the above. ν seems to be slightly larger than 0.587 for the most precise simulations with $w = 0.4$ and $w = 0.5$. Together with the SAW value we thus propose $\nu = 0.5872 \pm 0.0005$. This is somewhat smaller than the estimates from [4, 17], but compatible with them. We should stress it is hard to estimate errors since the values depend strongly on the parametrization chosen. Thus we conclude that explicit fits are useful, but somewhat dangerous.

The main disadvantage of the above procedure is that it requires explicit fits to

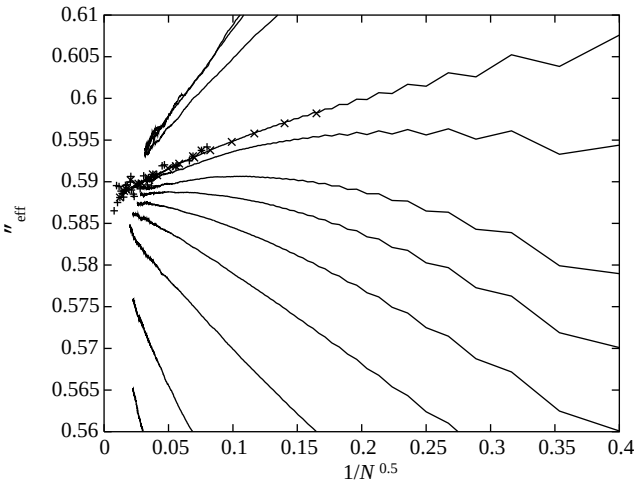

Figure 5. The effective exponent $\nu_{\rm eff}^{(e)}$ for different w, q. From above: $q = 1.0, 0.4, 0.2$; $w = 1.0, \ldots, 0.05$. Data for SAW ($w = 1.0$). $\times$, our pivot algorithm; $+$, from [4, 23].

nonuniversal parameters. As an alternative we can form expressions where all dependence on nonuniversal parameters disappears in the scaling limit. The simplest such combination is the ratio R_g^2/R_e^2. It is plotted against $1/\sqrt{N}$ in figure 4. In addition to our own data we show there also those of [4]. Apart from the obvious consistency of the data, the most remarkable observation is that the data approach the asymptotic value $R_g^2/R_e^2 = 0.159\,95 \pm 0.000\,10$ from above for $w < 0.4$, and from below for $w > 0.4$. This is fully compatible with the two-branch hypothesis and suggests that the transition between weak and strong coupling is at $w^* \approx 0.4$. But the strong curvatures seen for smaller N in the curves for $w \approx w^*$ indicate sizeable nonuniversal corrections to scaling, since R_g^2/R_e^2 should be constant for $w = w^*$ if such corrections were absent.

The next simple possibility is to study effective exponents. For ν, an obvious ansatz is

$$\nu_{\rm eff}^{(e)}(N) = \frac{1}{2\log a} \log\left[\frac{R_e(aN)}{R_e(N/a)}\right] \tag{23}$$

which according to the theory should tend to $\nu = 0.588$ for $\tilde{z} \to \infty$. The optimal choice of a depends on the balance between statistical errors and the range over which $\nu_{\rm eff}^{(e)}(N)$ can be estimated. The latter decreases if a is taken large, while the former diverge for $a \to 1$. In figure 5 we show results obtained with $a = \sqrt{2}$, plots with $a = 2$ are similar. Again we include older data for comparison. Again the most remarkable observation is that the data approach the asymptotic value ν from below for $w < 0.4$, and from above for $w > 0.4$. To understand this result we consider varying w and q for fixed N, say $N \approx 500$. If the couplings w, q are small we are concerned with an almost RW and $\nu_{\rm eff}^{(e)} \approx 0.5 < \nu$. Increasing the repulsion, one effect is to increase the effective stiffness of the walk. Indeed extending the repulsion range beyond nN, we could approximate a stiff rod, where $\nu_{\rm eff}^{(e)} = 1 > \nu$. It thus is plausible that $\nu_{\rm eff}$ tends to ν from above for large self repulsion, and vice versa. Again the leading corrections to scaling change sign at $w = w^* \approx 0.4$. But again we see strong curvature for $w = w^*$, indicating substantial nonuniversal corrections to scaling for $N < 400$.

To obtain a similar effective exponent $\gamma_{\rm eff}$, we have to take triple ratios instead of simple ratios as for $\nu_{\rm eff}$. This is due to the unknown critical fugacity μ^* in equation (19). The

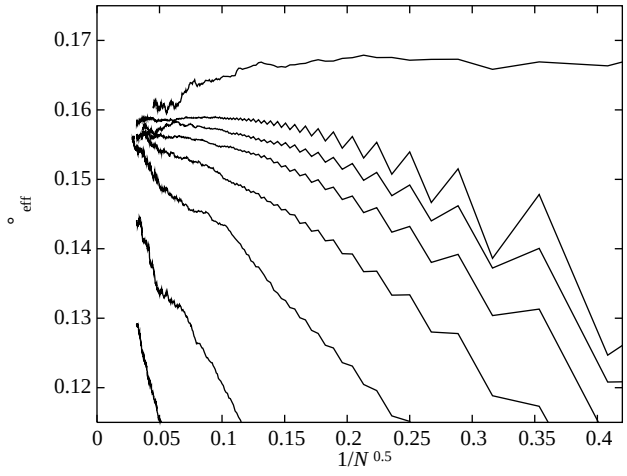

Figure 6. The effective exponent $\gamma_{\rm eff}$ for different w, q. From above: $q = 0.2$; $w = 1.0, 0.5, 0.4, 0.3, 0.2, 0.1, 0.05$.

general ansatz is thus

$$\gamma_{\rm eff}(N) = 1 + \frac{\log\left[\frac{C^x(aN)C^y(bN)}{C(N)}\right]}{[x\log a + y\log b]} \tag{24}$$

with

$$x + y = ax + by = 1 \qquad a < 1 < b. \tag{25}$$

The optimal choice for a and b depends now in addition on the way in which statistical errors increase with N. In the present case, they increase roughly as N^α with $\alpha \approx \frac{3}{4}$. In order to keep a large range in N we want the ratio b/a not to exceed 8. With this constraint one finds numerically that the minimal error of $\gamma_{\rm eff}(N)$ is obtained roughly for $a = \frac{1}{2}, b = 4$, giving $x = \frac{6}{7}, y = \frac{1}{7}$. Effective exponents obtained with this choice are shown in figure 6. The main conclusion from this plot is the same as from the previous ones: the two branches are visible with $w^* \approx 0.4$, but nonuniversal corrections to scaling cannot be neglected.

In terms of the function $F(\tilde z)$ (see (19)) $\gamma_{\rm eff}(\tilde z)$ reads

$$\gamma_{\rm eff}(\tilde z) = \gamma + \frac{7}{4\log 2}\left[\log F(\tilde z) - \frac{6}{7}\log F\left(\frac{\tilde z}{\sqrt{2}}\right) - \frac{1}{7}\log F(2\tilde z)\right] \tag{26}$$

and is only a function of $\tilde z$.

According to renormalization theory the end-to-end distance should obey the scaling law expressed in equation (2). In the next section we shall present detailed analyses of this and similar scaling laws, where we compare with the specific scaling functions predicted by perturbation theory. But the scaling law itself should hold independently of any perturbative arguments, and it seems worth while to test it without assuming any knowledge about the scaling function $\tilde\alpha_e(\tilde z)$. This is what we shall do now. The idea is the following: assume we know the parameters $\tilde l$ and $\tilde v$ for one pair of (w, q). Since our data overlap strongly, we can then obtain $\tilde l$ and $\tilde v$ for a neighbouring pair of (w, q) by demanding that the curves fall on top of each other in a scaling plot where $R_e\tilde l^{-1}N^{-1/2}$ is plotted against $\tilde z$. Actually, due to finite size corrections, we only demand that parabolic approximations coincide for large $\tilde z$. Finally, for the weak-coupling branch we can pin down the functions $\tilde l$, $\tilde v$ and $\tilde\alpha_e(\tilde z)$

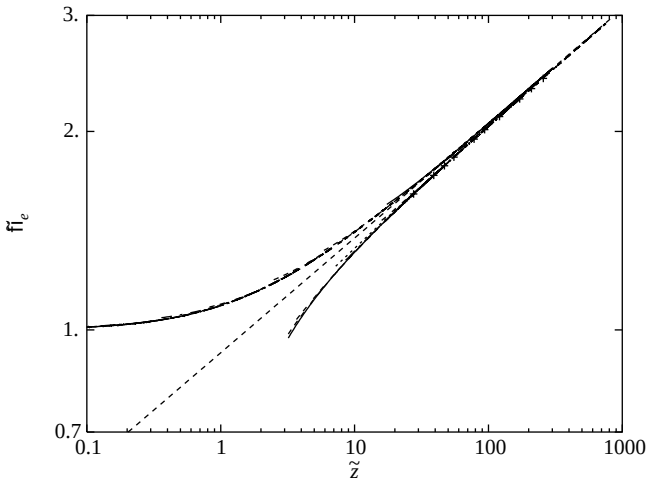

Figure 7. The empirical scaling function $\tilde{\alpha}_e$ as a function of $\tilde{z}$. The lower (strong coupling) branch can be shifted arbitrarily parallel to the diagonal, while the position of the upper (weak coupling) branch is fixed uniquely. $+$, are from our pivot simulations. Only data for $N \geqslant 10$ are shown. The broken curve is the asymptotic result, $\tilde{\alpha}_e \sim \tilde{z}^{2\nu-1}$.

Table 3. The parameters w and q and the resulting nonuniversal parameters.

w	q	$\tilde{v}_3$	$\tilde{l}$	$\tilde{v}$	f_0	b	μ^*
0.001 25	0.00	0.002 21	0.4082	0.002 16	0.002 16	1.001	1.791 123
0.002 50	0.00	0.004 51	0.4077	0.004 47	0.004 44	1.000	1.790 500
0.005 00	0.00	0.009 08	0.4073	0.009 07	0.008 97	0.999	1.789 282
0.010 00	0.00	0.018 3	0.4064	0.018 3	0.017 9	0.998	1.786 935
0.020 00	0.00	0.038 1	0.4043	0.038 2	0.036 5	0.995	1.782 544
0.050 00	0.00	0.103 6	0.3989	0.104 0	0.092 5	0.990	1.770 397
0.100 00	0.00	0.243	0.3894	0.244	0.189 4	0.983	1.752 666
0.200 00	0.00	0.697	0.3678	0.698	0.389 8	0.972	1.722 091
0.300 00	0.00	1.748	0.3374	1.777	0.606 2	0.960	1.695 241
0.400 00	0.00	5.884	0.2867	6.193	0.832 0	0.951	1.670 667
0.500 00	0.00	16.75	0.2567	15.11	1.096 2	0.940	1.648 037
0.600 00	0.00	5.066	0.3242	5.011	1.334 8	0.946	1.625 297
0.800 00	0.00	2.817	0.3842	2.790	1.808 1	0.988	1.583 981
1.000 00	0.00	2.324	0.4189	2.337	2.192 8	1.071	1.544 161
1.000 00	0.20	0.971	0.5409	0.971	2.398 0	0.219	1.501 752
1.000 00	0.40	0.839	0.5917	0.836	3.257 1	0.280	1.475 264
1.000 00	1.00	0.840	0.6607	0.841	3.935 7	0.413	1.398 156

completely by using the fact that the swelling factor $\tilde{\alpha}_e(\tilde{z}) \to 1$ for $\tilde{z} \to 0$. For the strong-coupling branch no such fixed point exists, and our scaling curve is arbitrary with respect to rescalings $\tilde{z} \to \lambda\tilde{z}$, $\tilde{\alpha}_e \to \lambda^{2\nu-1}\tilde{\alpha}_e$. Our results are shown in figure 7. They prove directly, *without using any explicit perturbative RG results*, the predicted two-branched structure. Furthermore, at least the weak-coupling branch agrees perfectly with equation (20). We should, however, admit that the latter is not very significant, more significant tests being given in the next section.

4. Comparison among theory and data

The previous analysis has shown the two-branched structure and the scaling of the swelling factor as predicted by renormalization theory. Now we compare the data with our quantitative one-loop calculation.

4.1. End-to-end swelling and parameter fitting

We first consider the effective exponent (23) which is expressed in terms of $\tilde{\alpha}_e^2(\tilde{z})$ as

$$\nu_{\rm eff}^{(e)}(\tilde{z}) = \frac{1}{2} + \frac{1}{4\log a}\log\left[\frac{\tilde{\alpha}_e^2(\sqrt{a}\tilde{z})}{\tilde{\alpha}_e^2(\tilde{z}/\sqrt{a})}\right]. \tag{27}$$

According to the theory it is a function of $\tilde{z}$ only and thus involves the single nonuniversal parameter $\tilde{v}$. Adjusting this parameter for each microstructure, i.e. each pair (w, q), we can bring the data onto the two branches as shown in figure 8. (Only the data with $N \geqslant 100$ were used in the fit.) Note that the theoretical curves are just covered by the data. The deviations seen are for chain lengths $N \lesssim 100$, as expected. Furthermore, the ranges of $\tilde{z}$ for different sets (w, q) strongly overlap, and scaling as a function of $\tilde{z}$ is clearly verified. The values of $\tilde{v}$ extracted are collected in table 1, row 3.

Turning now to the swelling factor $\tilde{\alpha}_e^2$ itself, we encounter the second parameter $\tilde{l}$. Allowing for a variation of both parameters $\tilde{v}$, $\tilde{l}$ simultaneously, we find the results similar to figure 7. Indeed, the empirical scaling function shown in figure 7 just coincides with the numerical evaluation of our one-loop result. The parameters are collected in table 1, rows 4 and 5. We note from equation (28), below, that $\tilde{v}$ should diverge for $f_0 \to 1$ (see also [8, figure 7]). Close to $f_0 = 1$ it therefore cannot be determined with high precision. Taking this into account we note that the results for $\tilde{v}$ from the two fits are fully consistent. (In the sequel we will use the values of the second fit.) We thus find full agreement among theory and data, verifying and strengthening the conclusions of [8].

As stressed above, the nonuniversal parameters $\tilde{l}$, $\tilde{v}$ cannot be calculated quantitatively from the microscopic model. However, as observed before [8], their variation can be

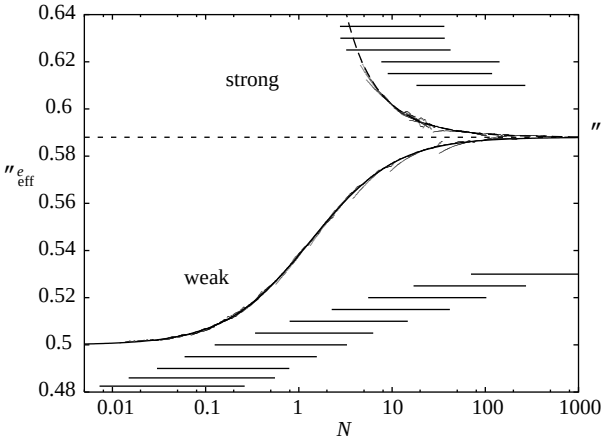

Figure 8. The effective exponent $\nu_{\rm eff}^{(e)}$ as a function of $\tilde{z}$. Data of the chain-growth algorithm. The curves give the result of the one-loop calculation. The horizontal lines indicate the intervals of $\tilde{z}$ for different w, q.

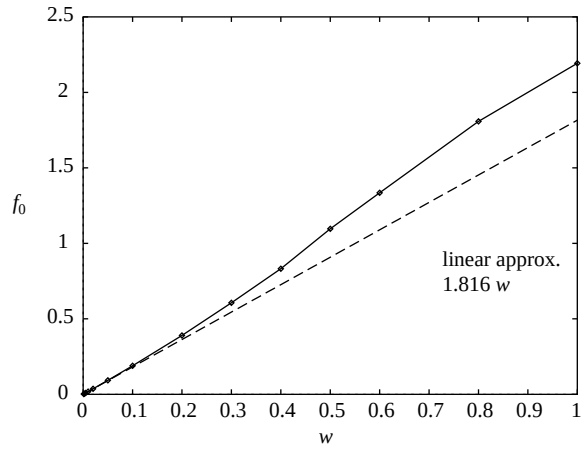

Figure 9. $f_0(w, 0)$ as a function of w for $q = 0$.

understood qualitatively from the RG mapping. Identifying in equation (7) ℓ_R with the microscopic cut-off ℓ and f with $f_0 = f_0(w, q)$ correspondingly, we have

$$\frac{\tilde{v}}{\tilde{l}} = \ell^{-1} f_0 |1 - f_0|^{-1/\omega} (1 + 0.824 f_0)^{0.25} \tag{28}$$

showing that $\tilde{v}/\tilde{l}$ diverges for $f_0 \to 1$. Furthermore for $\ell_R = \ell$ the relation

$$n_R = b(w, q) N \tag{29}$$

should hold, so that equation (8) yields a second relation

$$b(w, q) = f_0^{-2} |1 - f_0|^{1/(\omega\nu)} \frac{1 - 0.005 f_0 - 0.028 f_0^2 + 0.022 f_0^3}{\sqrt{1 + 0.824 f_0}} \tilde{v}^2. \tag{30}$$

Both $b(w, q)$ and $f_0(w, q)$ are expected to be smoothly varying functions of w and q, in contrast to the parameters $\tilde{l}$, $\tilde{v}$ of our two-parameter model, which are singular for $f_0 \to 1$. To test this idea, we transform the measured parameters $\tilde{v}$, $\tilde{l}$ ($q = 0$) to $f_0(w, 0)$, $b(w, 0)$ via equations (28) and (30). Figures 9 and 10 show the results. As expected, $f_0(w, 0)$ and $b(w, 0)$ vary smoothly. In particular,

$$f_0(w, 0) \approx \text{constant } w \tag{31}$$

holds for $w \lesssim 0.2$ to good approximation. $f(w^*, 0) = 1$ is found for $w^* \approx 0.47$. This value is slightly larger than the estimate $w \approx 0.4$ suggested by the analyses of section 3. The discrepancy might result from inaccuracies of the theoretical scaling functions or from $1/N$ corrections to scaling, but it is not very significant anyhow. The point $w = w^*$ (for $q = 0$) is similar to a critical point: the RG flow has a fixed point at the latter, while its projection onto the least-stable direction has a fixed point at w^*. Therefore, the leading corrections to scaling are absent at w^*, and all corrections should be due to $1/N$ effects. In agreement with earlier results the SAW belongs to the strong-coupling regime. The parameter $b(w, 0)$ varies only weakly, consistent with $b(w, 0) = 1 + \mathcal{O}(w)$.

We here should recall that traditionally the swelling factor is defined as

$$\alpha_e^2 = \frac{R_e^2}{R_{e,0}^2} = \frac{\tilde{l}^2}{\ell^2} \tilde{\alpha}_e^2 \tag{32}$$

where $R_{e,0} = R_e(f_0 = 0)$ is the end-to-end distance in the absence of the self repulsion. This differs from the universal swelling factor $\tilde{\alpha}_e^2$ due to the nonuniversal dependence $\tilde{l} = \tilde{l}(w, q)$.

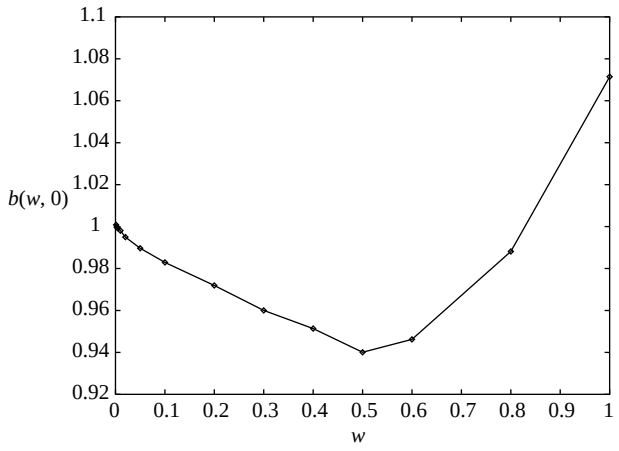

Figure 10. $b(w, 0)$ as a function of w for $q = 0$.

4.2. Other observables

Given $\tilde{v}$, $\tilde{l}$ from the analysis of R_e^2 we now can compare data for other quantities with the theoretical predictions. Figure 11 shows the result for $\gamma_{\text{eff}}(\tilde{z})$ constructed from the partition function according to equation (26). We find excellent agreement. Figure 12 shows our results for the effective exponent defined in terms of R_g:

$$\nu_{\text{eff}}^{(g)} := \frac{1}{2\log a} \log\left[\frac{R_g(aN)}{R_g(N/a)}\right]. \tag{33}$$

Again the agreement is excellent. Only on the strong-coupling branch are there some deviations for shorter N, indicating that $1/N$ corrections are more important for R_g than for R_e, as expected. Finally we note that a plot of the swelling factor $\tilde{\alpha}_g^2(\tilde{z})$ looks most similar to figure 7 for $\tilde{\alpha}_e^2(\tilde{z})$. Again scaling with a two-branched scaling function is nicely confirmed, but the theoretical curves are shifted by a small amount compared to the data. This is a familiar deficiency of the first-order approximation, which does not reproduce precisely the experimental value of the ratio R_e^2/R_g^2 in the excluded volume regime $\tilde{z} \gg 1$. It is too small by about 3%. It is well known that this small deviation is eliminated by a second-order calculation.

For shorter chains we expect deviations of experimental data from the theory, that should roughly behave as $1/N$, see equation (21). Our expectation is verified for all parameter values. For $q = 0$, $w \ll 1$ the deviation amplitude B is essentially zero. It increases with increasing w and reaches a maximum of ~ 0.1 around w^*, where we switch from the weak-coupling to the strong-coupling branch. Similar results are found for R_g, the amplitude being about three times larger than for R_e. This reflects the fact that R_g sums contributions from subchains of all sizes.

5. Conclusions

Our results show excellent agreement among Monte Carlo data and field theoretic predictions. Systematically varying the excluded volume strength we find that the data obey scaling as functions of $\tilde{z}$, exhibiting also the expected nonuniversal $1/N$-corrections. They quantitatively agree with field theory, provided we take the two-branched structure predicted

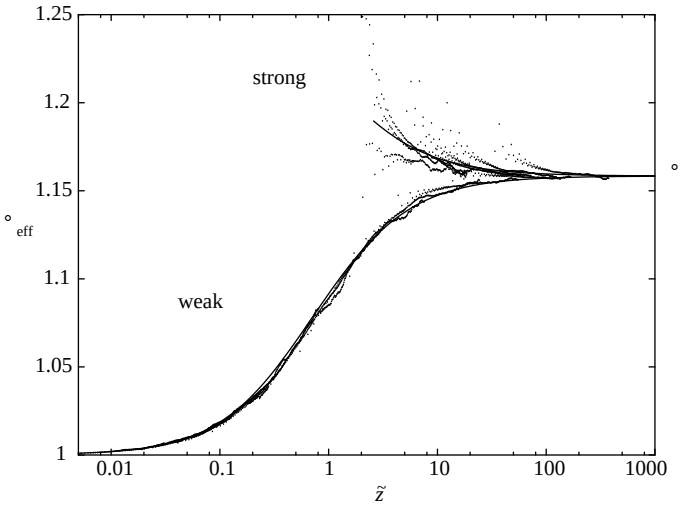

Figure 11. $\gamma_{\rm eff}$ as a function of $\tilde{z}$. The smooth curves give the theoretical result.

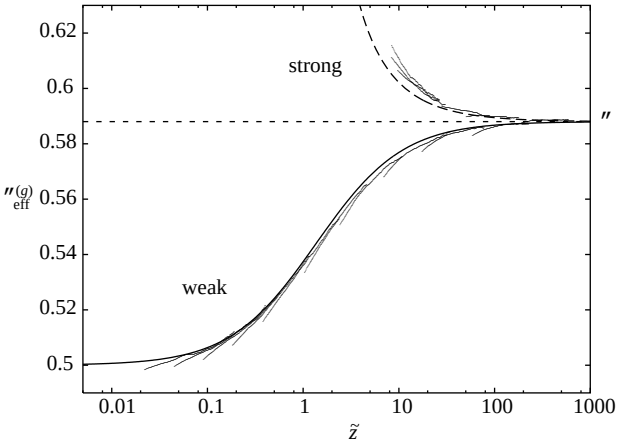

Figure 12. The scaling function $\nu_{\rm eff}^{(g)}$ as a function of $\tilde{z}$. The smooth curves give the theoretical result.

by the theory into account. This latter aspect is essential and is established here beyond doubt, even without involving the quantitative prediction of the one loop calculation. All our data are fully consistent with the two-parameter structure of the theory. Also the dependence of the parameters on the microstructure is consistent with qualitative theoretical ideas.

Previous MC analysis often came to the conclusion that only the asymptotic exponents are consistent with theoretical predictions, and that the variation outside the excluded volume limit is not covered by the theory. The present work shows that this pessimistic view is erroneous.

Note added in proof. In a recent preprint Caracciolo S *et al* (cond-mat 9703250) have used the pivot algorithm for a high precision estimate of the exponent γ. Their result $\gamma = 1.1575 \pm 0.0006$ is in very good agreement with our present estimate and shows that the pivot algorithm is also efficient for this purpose.

Acknowledgment

This work was supported by the Deutsche Forschungsgemeinschaft through Sonderforschungsbereich 237.

References

[1] Brézin E, Guillou J C, and Zinn-Justin J 1976 *Phase Trasitions and Critical Phenomena* vol VI, ed C Domb and M S Green (New York: Academic)
[2] Liu A J and Fisher M E 1990 *J. Stat. Phys.* **58** 431
[3] Nickel B G 1991 *Macromolecules* **24** 1358
[4] Li B, Madras N and Sokal A D 1995 *J. Stat. Phys.* **80** 661
[5] Sokal A D 1994 *Europhys. Lett.* **27** 661
[6] Bagnuls C and Bervillier C 1990 *Phys. Rev.* B **41** 402
[7] Bagnuls C and Bervillier C 1994 *preprint*, see also *Phys. Lett.* **195A** 163
[8] Schäfer L 1994 *Phys. Rev.* E **50** 3517
[9] Krüger B and Schäfer L 1996 *Macromolecules* **29** 4737
[10] Domb C and Joyce G S 1972 *J. Phys. C: Solid State Phys.* **5** 956
[11] Hegger R and Grassberger P 1994 *J. Phys. A: Math. Gen.* **27** 4069
[12] Grassberger P 1997 *Phys. Rev.* E to be published
[13] Müller S and Schäfer L 1997 *preprint*
[14] Schloms R and Dohm V 1989 *Nucl. Phys.* B **328** 639
[15] Krüger B and Schäfer L 1994 *J. Physique* I **4** 757
[16] Schäfer L 1997 *Excluded Volume Effects in Polymer Solutions* (Springer) to be published
[17] Le Guillou J C and Zinn-Justin J 1989 *J. Physique* **50** 1365
[18] Hughes B D 1995 *Random Walks and Random Environments* vol 1 (Oxford: Clarendon) p 487
[19] Yamakawa H, Abe F and Einaga Y 1993 *Macromolecules* **26** 1898
[20] Cotton J P 1988 *J. Phys. Lett. France* **41** 231
[21] des Cloizeaux J and Jannink G 1990 *Polymers in Solution* (Oxford: Clarendon)
[22] Madras N and Sokal A D 1988 *J. Stat. Phys.* **50** 109
[23] Nickel B unpublished data quoted in A J Barrett *et al* 1991 *Macromolecules* **24** 1615
[24] Eizenberg N and Klafter J 1993 *J. Chem. Phys.* **99** 3976
[25] Zifferer G 1990 *Macromolecules* **23** 3166
[26] Caracciolo S, Pelissetto A and Sokal A D 1992 *J. Stat. Phys.* **67** 65
[27] MacDonald D, Hunter D L, Kelly K and Jan N 1992 *J. Phys. A: Math. Gen.* **25** 1429
[28] Grassberger P 1993 *J. Phys. A: Math. Gen.* **26** 2769